

---

# A DYNAMIC MEMORY ASSIGNMENT STRATEGY FOR DILATION-BASED ICP ALGORITHM ON EMBEDDED GPUS

---

**Qiong Chang**  
School of Computing  
Institute of Science Tokyo  
Tokyo, Japan 152-8550  
q.chang@c.titech.ac.jp

**Weimin Wang**  
Dalian University of Technology  
Dalian, China 210093  
wangweimin@dlut.edu.cn

**Junpei Zhong**  
University of Wollongong (College HK)  
Hong Kong, China  
joni.zhong@ieee.org

**Jun Miyazaki**  
School of Computing  
Institute of Science Tokyo  
Tokyo, Japan 152-8550  
miyazaki@c.titech.ac.jp

December 5, 2025

## ABSTRACT

This paper proposes a memory-efficient optimization strategy for the high-performance point cloud registration algorithm VANICP, enabling lightweight execution on embedded GPUs with constrained hardware resources. VANICP is a recently published acceleration framework that significantly improves the computational efficiency of point-cloud-based applications. By transforming the global nearest neighbor search into a localized process through a dilation-based information propagation mechanism, VANICP greatly reduces the computational complexity of the NNS. However, its original implementation demands a considerable amount of memory, which restricts its deployment in resource-constrained environments such as embedded systems. To address this issue, we propose a GPU-oriented dynamic memory assignment strategy that optimizes the memory usage of the dilation operation. Furthermore, based on this strategy, we construct an enhanced version of the VANICP framework that achieves over 97% reduction in memory consumption while preserving the original performance. Source code is published on: <https://github.com/changqiong/VANICP4Em.git>.

## 1 Introduction

The Iterative Closest Point (ICP) algorithm is one of the most fundamental methods in 3D vision, widely used for point cloud registration in tasks such as tracking [1], and object recognition [2, 3]. However, ICP is computationally intensive, as its performance is dominated by the time-consuming nearest neighbor search (NNS) process [4]. Recently, many studies have focused on accelerating point cloud registration to enhance its applicability in real-world scenarios [5, 6]. Alexander [7] proposed a multi-GPU strategy that efficiently performs nearest neighbor search on large-scale point clouds. Yu et al. [8] employed a Hierarchical Navigable Small World (HNSW) structure to accelerate descriptor matching within their point cloud alignment framework. More recently, VANICP [9] demonstrates significant performance gains by transforming the global NNS into a localized process through a dilation-based strategy. It completes the registration of the *Stanford bunny* dataset (containing over 40k points) within 0.5s on an RTX 3080 GPU. However, it still suffers from a critical limitation that requiring preallocating a large and fixed memory space (approximately 2GB) to support voxel dilation operations across regions with varying sparsity. This leads to two major challenges: 1), the substantial memory consumption renders the framework unsuitable for embedded systems, where computational resources, energy budgets, and mobility are tightly constrained; 2), the fixed-size memory allocation lacks adaptability, which may result in either significant memory waste or insufficient capacity under different datasets.

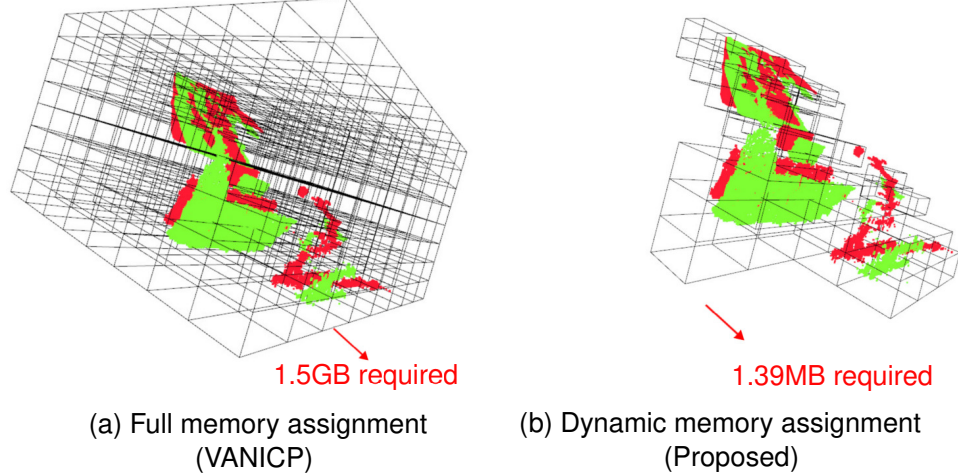


Figure 1: Comparison of memory consumption in dilation. For the *TUM* model (226K points), the original VANICP adopts a monolithic contiguous assignment strategy for dilation, which supports direct addressing. In contrast, the proposed method employs a segmented pointer-based assignment strategy that relies on indirect addressing.

To overcome the above challenges, we proposed a GPU-oriented dynamic memory assignment strategy tailored for embedded GPU platforms. Leveraging the unified memory of embedded GPUs, the proposed strategy dynamically allocates memory for each voxel in a heterogeneous manner based on the number of points contained within it. Specifically, the method performs parallel counting of points in each voxels, followed by a serial computation of memory start addresses to ensure correct allocation boundaries. Experimental results demonstrate that the proposed strategy reduces memory consumption by more than 97%, while maintaining the original computational performance of VANICP.

The remainder of this paper is organized as follows. Section II introduces the original VANICP algorithm and outlines its core principles. Section III presents the proposed GPU-oriented dynamic memory assignment strategy and its implementation details. Section IV describes the experimental setup and discusses the results. Section V reviews related approaches for accelerating ICP algorithms. Finally, Section VI concludes the paper by summarizing the key contributions and outlining potential directions for future work.

## 2 Background

### 2.1 VANICP

The goal of the basic ICP is to align a source point cloud  $P = \{p_1, p_2, \dots, p_m\}$  with a target point cloud  $Q = \{q_1, q_2, \dots, q_n\}$  by iteratively estimating a rigid transformation between them. In each iteration, correspondences are first established by finding the nearest neighbor  $q'_i$  for each source point  $p_i$ . And then, ICP estimates the optimal rotation matrix  $R \in \mathbb{R}^{3 \times 3}$  and the translation vector  $t \in \mathbb{R}^3$  that minimize the mean squared error function between the corresponding pairs:

$$\min_{R, t} \sum_i \|R p_i + t - q'_i\|^2. \quad (1)$$

As the most computationally intensive step of the ICP, the nearest neighbor search (NNS) has attracted considerable attention from researchers seeking performance optimization. Among the proposed acceleration methods, VANICP [9, 10] distinguishes itself with a unique dilation-based design that transforms the global NNS into a localized process. This design enables substantially higher performance compared to traditional kd-tree-based registration methods [11]. In VANICP, the accelerated NNS can be decomposed into the following phases:

**Step1: Voxelization** The target point cloud is first converts into a discrete 3D grid structure, where the space is divided into small voxels. Each voxel contains all points that fall within its spatial boundary, effectively grouping nearby points together. This structured representation facilitates efficient spatial indexing and reducing the computational cost of subsequent nearest neighbor searching.

**Step2: Voxel Dilation** This step is applied during early iterations when the overlap between source and target point clouds is still limited. By dilating the occupied voxels, the algorithm effectively enlarges the overlap region, enabling more source points to find valid correspondences within nearby target voxels. This not only improves matching

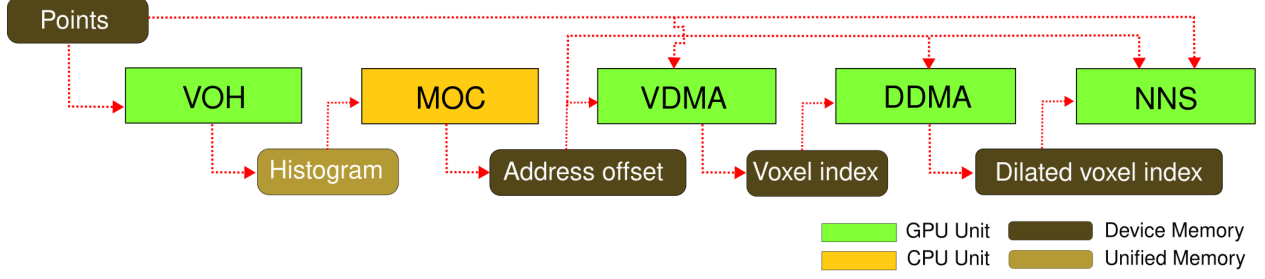


Figure 2: Processing flow of the proposed framework. VOH: voxelization occupancy histogram. MOC: memory offset computation. VDMA: voxelization with dynamic memory assignment. DDMA: dilation with dynamic memory assignment. NNS: nearest neighbor searching. This strategy first performs voxel-wise histogram construction on the GPU to parallelize point counting, and then computes the memory offset of each voxel on the CPU via unified memory. By integrating offset-based indexing into subsequent processing stages, it significantly reduces the overall memory utilization.

robustness in the initial stages but also accelerates the propagation of spatial information across adjacent regions, leading to faster and more stable convergence.

**Step3: Local Approximate Nearest Neighbor Search** After voxelization and dilation, each source point only needs to search within its assigned voxel or its dilated neighbors, rather than across the entire target point cloud. If the voxel is non-empty, a local search is performed ( $O(n)$  complexity within the voxel). If the voxel is empty, the algorithm falls back to a global search to ensure correctness, though such cases become increasingly rare as iterations proceed.

Finally, the nearest neighbor search of each source point is mapped to an individual GPU thread. Leveraging voxel-based locality, these approximate nearest neighbor searches are highly parallelizable, avoiding the global kd-tree traversals or brute-force distance computations that dominate traditional ICP.

## 2.2 Memory Inefficiency Caused by Voxel Sparsity Variations

Since the dilation operation is performed voxel-wise in parallel, each voxel requires an independent memory block. However, voxels often exhibit significant sparsity because the number of points they contain varies widely. Ideally, memory allocation should be dynamic, scaling with the actual number of points in each voxel. In practice, however, GPUs are optimized for massive parallelism and deterministic resource management, relying on preallocated, contiguous memory regions to sustain high throughput and minimize synchronization overhead. Consequently, VANICP adopts a static strategy that preallocates a 64KB memory block per voxel. This approach not only causes substantial memory waste since many voxels contain only a few points, but also limits adaptability to point clouds of varying density and scale. Furthermore, the large memory utilization makes the framework unsuitable for embedded systems, where computational resources and energy efficiency are tightly constrained.

## 3 Proposed Algorithm

In this section, we plan to introduce the proposed dynamic memory assignment strategy.

Figure 2 illustrates the overall pipeline of the proposed strategy. Unlike VANICP, which assigns a fixed memory size to each voxel, our approach dynamically allocates memory according to the actual occupancy of the input point cloud. In addition to the voxelization, dilation, and NNS stages inherited from VANICP, we introduce a series of preprocessing steps that leverage heterogeneous computation to gather voxel-wise statistics. Specifically, a parallel histogram is constructed on the GPU to count the number of points in each voxel, followed by a prefix-based computation of the voxel memory offsets on the CPU. By exploiting the unified memory of embedded GPUs, both histogram construction (parallel) and offset accumulation (serial) can be performed efficiently within a single address space. The memory offset plays a crucial role in this strategy. Since it is derived from the point count of each voxel, the offset implicitly encodes both the size of each voxel and the total memory requirement. Instead of the original direct-addressing strategy that relies on a monolithic memory layout, the proposed method adopts an indirect-addressing approach through the memory offset. Although this introduces additional memory accesses, the overhead is outweighed by the nearly 100x reduction in memory utilization.

**Algorithm 1:** Heterogeneous Address Offset Computation

---

```

// GPU-side Voxel Occupancy Histogram Generation
Input: Target point  $P_i$ 
Output: VoxelHist
1 foreach point  $P_i$  do
2    $V_x, V_y, V_z \leftarrow \text{Quantize}(P_i.x, P_i.y, P_i.z)$ 
3    $\text{IndexVoxel} \leftarrow \text{Concat}(V_x, V_y, V_z)$ 
4    $\text{key} \leftarrow \text{IndexVoxel} \& (\text{BLOCK\_SIZE} - 1)$ 
5   while True do
6      $\text{prev} \leftarrow \text{atomicCAS}(\text{SMem}[\text{key}], 0, \text{IndexVoxel} < 16)$ 
7     if  $(\text{prev} == 0) \vee ((\text{prev} \gg 16) == \text{IndexVoxel})$  then
8        $\text{atomicAdd}(\&\text{SMem}[\text{key}], 1)$ 
9       break
10     $\text{key} \leftarrow (\text{key} + 1) \& (\text{BLOCK\_SIZE} - 1)$ 
11   $\text{syncthreads}()$ 
12  if  $\text{SMem}[\text{threadIdx.x}] == 0$  then
13     $\text{atomicAdd}(\&\text{VoxelHist}[\text{SMem}[\text{threadIdx.x}] \gg 16], \text{SMem}[\text{threadIdx.x}] \& 0\text{XFFFF})$ 
14
// CPU-side Memory Offset Computation
Input: VoxelHist
Output: AddrOffset
15  $\text{HeadAddr} \leftarrow 0$ 
16 foreach  $\text{VoxelIndex} \in \text{VoxelNumber}$  do
17    $\text{cnt} \leftarrow (\text{VoxelHist}[\text{VoxelIndex}] == 0) ? 2 : \text{VoxelHist}[\text{VoxelIndex}] + 2$ 
18    $\text{VoxelHist}[\text{VoxelIndex}] \leftarrow \text{HeadAddr}$ 
19    $\text{HeadAddr} \leftarrow \text{HeadAddr} + \text{cnt}$ 
20  $\text{Memcpy}(\text{AddrOffset}, \text{VoxelHist})$ 

```

---

Algorithm 1 illustrates the pseudocode for address offset generation. The heterogeneous design is motivated by two considerations: (1) the voxel occupancy histogram can be efficiently constructed in parallel on GPUs, while the dilation offsets must explicitly distinguish between empty and non-empty voxels that can be handled more flexibly on the CPU; (2) on embedded platforms, unified memory architectures provide higher effective bandwidth and lower coordination overhead than discrete GPUs. It worth to be noted that, since the cost of atomic operations on embedded GPUs is significantly higher than discrete GPUs, constructing a histogram through the global memory directly is not a good choice. Therefore, we propose a two-layer memory structure based on a variant hash table strategy to reduce atomic conflicts in global memory. Concretely, the points are first voxelized according to their spatial coordinates (lines 2,3). We then derive hash keys from these voxel indices and construct a hash table for each block in shared memory (lines 4-11). To avoid additional memory overhead that may reduce thread parallelism, the hash key and value are compactly encoded into a single 32-bit entry, with the upper 16 bits storing the key and the lower 16 bits storing the value. This fused representation allows us to count the number of points while preserving the original voxel index information. After the hash tables are filled, each thread extracts the entries from non-empty hash slots and adds them to global memory, where a global histogram over all voxels is subsequently constructed (lines 12, 13). Based on the histogram, the address offset of each voxel is then accumulated according to the number of points it contains (lines 15-19). To save the memory consumption, the offset values are updated in place directly on the histogram. Furthermore, two additional segments are allocated for each voxel to ensure correct parallel execution of the subsequent dilation step (Figure 3). Finally, the address offsets are copied into the device memory region (line 20), since the offsets will be frequently accessed by subsequent GPU kernels.

Algorithms 2–4 detail the voxelization, dilation, and nearest neighbor search (NNS) procedures under the proposed dynamic memory assignment strategy. They inherit the core computational design of VANICP, but employ a different memory access strategy. VANICP achieves high throughput through a monolithic memory policy, in which all point data are consolidated during the voxelization stage into a single block, enabling dilation and NNS to be executed by direct addressing. In contrast, the proposed method adopts a segmented pointer-based assignment strategy, where points are accessed indirectly through the index without being merged into a unified memory space (line 8 in Algorithm 2). This design substantially reduces the memory utilization while preserving computational efficiency, as it eliminates the need for data replication. Figure 3 illustrates the overall memory assignment strategy. The address offset, dilated voxel

**Algorithm 2:** Voxelization under Dynamic Memory Assignment**Input:** Target point  $P_i$ , AddrOffset**Output:** VoxelMem

---

```

1  $V_x, V_y, V_z \leftarrow \text{Quantize}(P_i.x, P_i.y, P_i.z)$ 
2  $VoxelIndex \leftarrow \text{Concat}(V_x, V_y, V_z)$ 
3  $VoxelAddr \leftarrow \text{AddrOffset}[VoxelIndex]$ 
4  $lock \leftarrow \text{True}$ 
5 while  $lock$  do
6   if  $\text{atomicCAS}(VoxelMem[VoxelAddr], 0, 1) == 0$  then
7      $count \leftarrow VoxelMem[VoxelAddr + 1]$ 
8      $VoxelMem[VoxelAddr + count + 2] \leftarrow \text{PointIndex}$ 
9      $VoxelMem[VoxelAddr + 1] \leftarrow count + 1$ 
10     $\text{atomicExch}(VoxelMem[VoxelAddr], 0)$ 
11     $lock \leftarrow \text{False}$ 

```

---

**Algorithm 3:** Dilation under Dynamic Memory Assignment**Input:** VoxelMem, AddrOffset**Output:** VoxelMem (dilated voxel memory)

---

```

1 for  $iter \leftarrow 0$  to  $DilationNumber$  do
2    $VoxelAddr \leftarrow \text{AddrOffset}[VoxelIndex]$ 
3   if  $VoxelMem[VoxelAddr + 1] \neq 0$  then
4      $DilationAddr \leftarrow \text{AddrOffset}[VoxelIndex + k]$  //  $k \in \{\pm 1, \pm 2^N, \pm 2^{2N}\}$ 
5     if  $\text{atomicCAS}(VoxelMem[DilationAddr], 0, 1) == 0$  then
6       if  $VoxelMem[DilationAddr + 1] == 0$  then
7          $VoxelMem[DilationAddr + 1] \leftarrow \text{Mask}(VoxelIndex)$ 

```

---

index, and points are stored in three separate memory spaces while maintaining their logical dependencies (highlighted in green and yellow). In contrast to VANICP’s static assignment strategy, the proposed design exploits the address offset structure to achieve dynamic and memory compact assignment (e.g. red-boxed area). To avoid race conditions during the dilation stage, a *Thread Lock* is associated with each voxel. During dilation, each voxel expands toward its six neighboring directions. If a neighboring voxel is initially empty, the index of the root voxel is bitwise-masked and retained until the NNS stage, after which it is released (lines 3-7 in Algorithm 3). The NNS is then performed directly

**Algorithm 4:** Fast Nearest Neighbor Search**Input:** VoxelMem, AddrOffset, TargetSet, SourceSet**Input:** Best\_Dist, Best\_Index

---

```

1  $V_x, V_y, V_z \leftarrow \text{Scale}(S.x, S.y, S.z)$ 
2  $VoxelIndex \leftarrow \text{Concat}(V_x, V_y, V_z)$ 
3  $VoxelAddr \leftarrow \text{AddrOffset}[VoxelIndex]$ 
4  $checkpoint \leftarrow VoxelMem[VoxelAddr + 1]$ 
5  $IndexRelease \leftarrow \text{Unmask}(checkpoint)$ 
6 if  $IndexRelease$  is DilatedVoxel then
7    $VoxelAddr \leftarrow \text{AddrOffset}[IndexRelease]$ 
8    $count \leftarrow VoxelMem[VoxelAddr + 1]$ 
9 else
10   $count \leftarrow checkpoint$ 
11 if  $count == 0$  then
12   foreach  $P_i \in \text{TargetSet}$  do
13      $Best\_Dist, Best\_Index \leftarrow \text{Globalsearch}(S, P_i)$ 
14 else
15   for  $i \leftarrow 0$  to  $count - 1$  do
16      $P_i \leftarrow \text{TargetSet}[VoxelMem[VoxelAddr + 1 + i]]$ 
17      $Best\_Dist, Best\_Index \leftarrow \text{Localsearch}(S, P_i)$ 

```

---

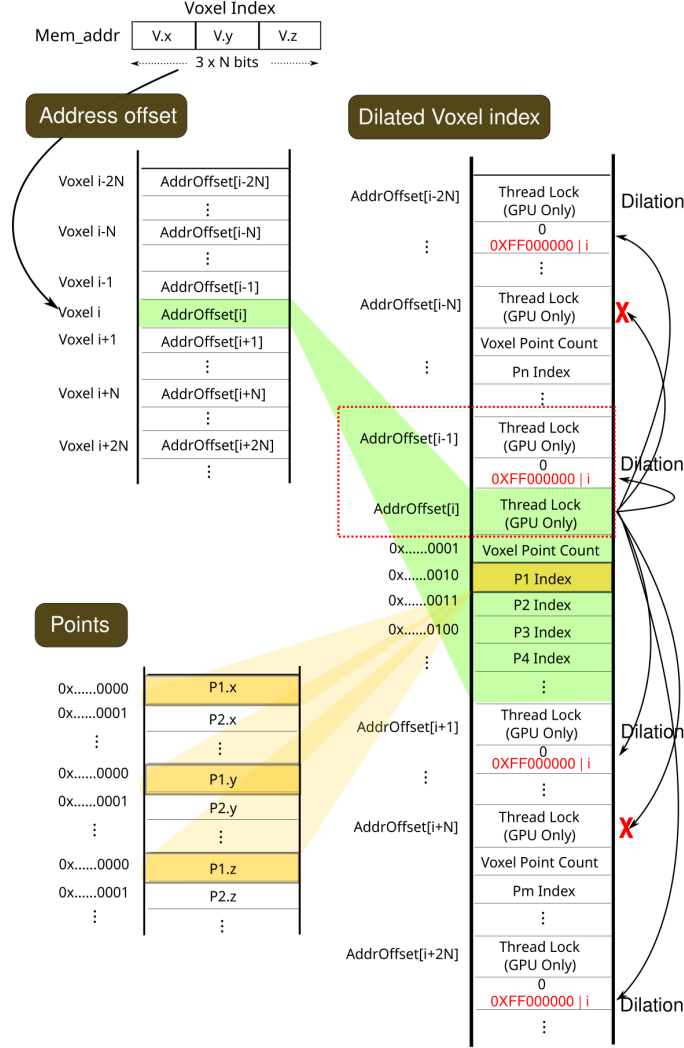


Figure 3: Memory assignment of the proposed strategy.

on the voxel index memory. The source points are first voxelized and mapped to their corresponding voxel regions by an address-offset lookup (lines 1-3 in Algorithm 4). Each voxel entry is subsequently examined by unmasking its state to determine whether it is dilated. If not, a localized NNS is conducted using only the point indexes within that voxel. Otherwise, the algorithm traces back to the associated root voxel through its index linkage (lines 4-10). When the voxel remains empty, it indicates that the boundary region of the space has not been fully filled, requiring a fallback to a global search. Since such boundary cases occur infrequently and involve only a small number of points, their overall impact on runtime performance is negligible (lines 11-17).

## 4 Experiments

This section presents the experimental setup and a series of comparative evaluations. Specifically, we benchmark performance across multiple datasets on various platforms, including ARM, embedded GPU and FPGA.

### 4.1 Experimental Setup

**Platform** We employ the Jetson AGX Xavier embedded GPU as the primary experimental platform. Built on the Volta architecture, it features 512 CUDA cores, providing strong parallel compute capability for edge workloads. The module integrates 32 GB of LPDDR4x memory with a bandwidth of up to 137 GB/s and supports GPU boost frequencies of approximately 1.37 GHz. Its unified global memory design allows the CPU and GPU to access shared memory

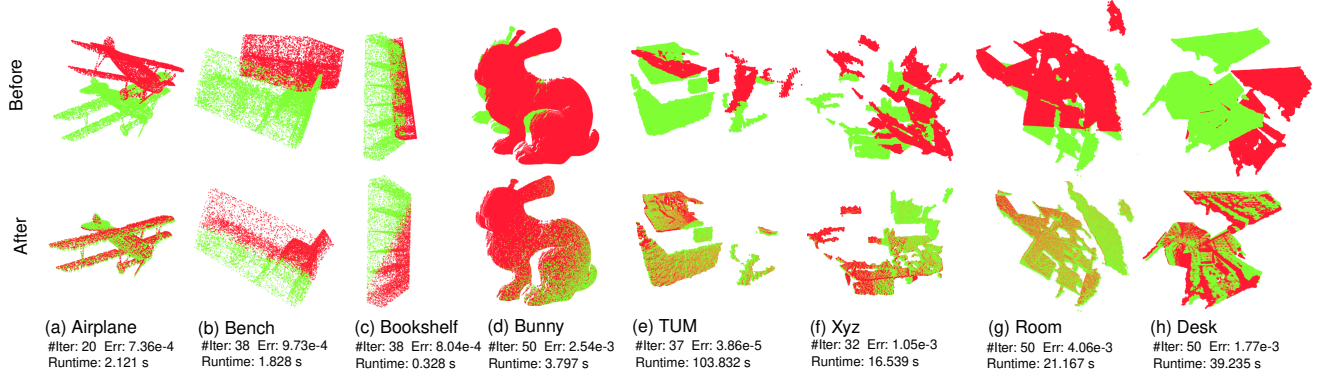


Figure 4: Registration results of the dilation-based ICP applied to the source point cloud (red) and the target point cloud (green).

without explicit data-copy operations, making the platform highly suitable for real-time and memory-constrained embedded applications. Additionally, for comparison, we also implemented our method on the Xilinx Zynq UltraScale+ MPSoC EV-series FPGA platform. It integrates a heterogeneous architecture consisting of a Processing System (PS) and Programmable Logic (PL). The PS includes four ARM Cortex-A53 cores operating at up to 1.2 GHz with a two-level cache hierarchy, while the PL offers 88 K lookup tables, 176 K flip-flops, and 4.5 MB of on-chip BRAM for custom hardware acceleration.

**Dataset** We evaluated our method on three point cloud datasets of different scales: *ModelNet* [12] with an average of 10k points, the *Stanford Bunny* [13] with approximately 40k points, and the *TUM RGB-D* dataset [14] containing over 200k points. These datasets are widely used in point cloud processing research and offer strong benchmarking value for performance assessment. All point clouds were normalized to fit within a unit sphere, and random perturbations were applied following the same protocol as the original VANICP [9].

**Parameter** In dilation-based ICP registration, four parameters play essential roles: the voxelization scale  $N$ , the number of dilation layers  $L$ , the maximum iteration count and the *RMSE* difference, both of which serve as convergence thresholds. The number of voxels along each dimension is  $2^N$ . VANICP is highly sensitive to  $N$  because it directly determines voxel-wise memory assignment. In contrast, our method is only weakly influenced by this parameter; therefore, we fix  $N = 4$  in our experiments. The parameter  $L$  is inversely related to  $N$ : a smaller voxel size requires more dilation steps to adequately cover the entire space, vice versa. Accordingly, we set  $L = 10$ . The maximum iteration count and the *RMSE* difference thresholds are set to 50 and  $1 \times e^{-5}$ , respectively, to ensure stable convergence across all tested datasets.

Table 1: Memory and Energy Consumption Analysis

| Dataset         | GPU Mem. (MB)     |        | Saving       | Runtime               |               |                 | Power(w) <sup>3</sup> |         |         |         | EC(J/F) <sup>4</sup> |        | Saving        |
|-----------------|-------------------|--------|--------------|-----------------------|---------------|-----------------|-----------------------|---------|---------|---------|----------------------|--------|---------------|
|                 | Ours <sup>1</sup> | VANICP |              | MOC <sup>2</sup> (ms) | Ours Total(s) | VANICP Total(s) | SYS_GPU               | SYS_SOC | SYS_CPU | SYS_DDR | Ours                 | VANICP |               |
| AirPlane (10k)  | 0.135             | 10     | <b>98.6%</b> | 0.251                 | 2.12          | 2.089           | 0.458                 | 1.07    | 0.458   | 0.152   | 4.7                  | 6.23   | <b>24.5%</b>  |
| Bench (10k)     | 0.135             | 6.25   | <b>97.8%</b> | 0.207                 | 1.83          | 2.156           | 0.763                 | 2.29    | 2.28    | 0.458   | 4.94                 | 5.9    | <b>16.4%</b>  |
| Bookshelf (10k) | 0.135             | 5      | <b>97.3%</b> | 0.328                 | 2.3           | 2.07            | 0.763                 | 2.138   | 1.832   | 0.458   | 6.122                | 5.84   | -4.1%         |
| Bunny (40k)     | 0.307             | 75     | <b>99.6%</b> | 0.399                 | 3.8           | 2.356           | 7.771                 | 3.2     | 0.913   | 0.913   | 11.48                | 10.417 | -10.2%        |
| TUM (226k)      | 1.39              | 1508   | <b>99.9%</b> | 1.29                  | 103.8         | 156.01          | 9.74                  | 3.65    | 0.608   | 1.065   | 330.7                | 471.74 | <b>29.8%</b>  |
| Xyz (229k)      | 1.39              | 312    | <b>99.5%</b> | 1.27                  | 16.54         | 28.477          | 9.29                  | 3.351   | 0.913   | 0.761   | 50.675               | 84.94  | <b>40.34%</b> |
| Room (239k)     | 1.39              | 381    | <b>99.6%</b> | 1.34                  | 21.17         | 49.85           | 9.14                  | 3.352   | 0.609   | 0.761   | 64.01                | 154.73 | <b>58.63%</b> |
| Desk (250k)     | 1.53              | 450    | <b>99.6%</b> | 1.42                  | 39.2          | 73.42           | 9.9                   | 3.351   | 0.456   | 0.761   | 118.64               | 224.95 | <b>47.2%</b>  |

<sup>1</sup> Static memory utilization for the **Histogram** and **Address offsets**: 0.03125 MB + dynamic memory utilization of the **Dilated Voxel Index**. <sup>2</sup>: Memory offset computation. <sup>3</sup>: Power consumption of GPU, CPU, SoC and memory. <sup>4</sup>: Energy consumption of the entire system per frame.

## 4.2 Experimental Results

We selected eight representative models from three datasets, covering a broad range of point counts, sparsity levels, and initial spatial poses. Figure 4 shows the registration results obtained using our proposed strategy. As the model size increases, both the number of iterations and registration time increase accordingly. Although the registration time and accuracy exhibit minor variations due to differences in initial poses, our strategy demonstrates strong robustness. In all cases, the source point cloud (red) successfully converges to the target (green).

Table 2: Performance comparison across multiple platforms

| Dataset           | Methods     | Hardware <sup>1</sup> | Runtime(s)  | Speedup     | Error          |
|-------------------|-------------|-----------------------|-------------|-------------|----------------|
| ModelNet<br>(10k) | FRICP[15]   | ARM                   | 0.17        | 1x          | 2.08e-6        |
|                   | Brute       | EmGPU                 | 2.5         | 0.07x       | <b>5.08e-7</b> |
|                   | KD-tree[16] | EmGPU                 | 5.35        | 0.03x       | 9.9e-5         |
|                   | VANICP[9]   | EmGPU                 | 2.089       | 0.08x       | 5.4e-4         |
|                   | Ours        | FPGA                  | <b>0.12</b> | <b>1.4x</b> | 1.38e-3        |
|                   |             | EmGPU                 | 2.121       | 0.08x       | 7.36e-4        |
| Bunny<br>(40k)    | FRICP[15]   | ARM                   | 15.2        | 1x          | 3.05e-3        |
|                   | KD-tree[16] | EmGPU                 | 8.1         | 1.87x       | <b>1.28e-4</b> |
|                   | Brute       | EmGPU                 | 5.01        | 3x          | 8e-3           |
|                   | VANICP[9]   | EmGPU                 | 3.356       | 4.5x        | 9e-3           |
|                   | Ours        | FPGA                  | <b>0.6</b>  | <b>25x</b>  | 1.47e-2        |
|                   |             | EmGPU                 | 3.793       | 4x          | 2.54e-3        |

<sup>1</sup> **ARM**: Cortex-A53. **EmGPU**: Jetson AGX Xavier. **FPGA**: Zynq UltraScale+ MPSoC EV.

Table 1 summarizes the memory and energy consumption of different models on the Jetson AGX Xavier GPU, including GPU memory utilization, runtime, and power consumption. For comparison, we also report the results obtained by VANICP. Our strategy comprises two memory components: a static footprint for the Histogram and Address Offsets (0.03125MB), and a dynamic footprint for the Dilated Voxel Index. Even for large-scale point clouds such as *Desk* with 250k points, the total memory required for dilation is only 1.53MB. In contrast, VANICP employs a static memory allocation strategy without voxel-wise adaptivity, necessitating a large pre-allocated memory space to guarantee successful dilation. For large and spatially non-uniform point clouds (e.g., *TUM*), the memory size even exceeds 1.5GB. Consequently, our dynamic memory assignment strategy reduces memory utilization by more than 97%. Notably, our dynamic memory assignment strategy does not incur additional computational overhead, as the memory-offset computation (MOC) consistently remains below 2ms. For small point clouds (fewer than 40k points), the runtime of our strategy is comparable to that of VANICP. For large-scale point clouds, the registration time of VANICP even increases, since points that exceed the voxel capacity force the algorithm to fall back to global registration. The *Power* and *EC* columns summarize the power consumption of each model on embedded GPU, including the GPU, CPU, SoC, and DDR memory, as well as the energy consumed per frame. Power consumption increases proportionally with the size of the point cloud model. Overall, our system exhibits slightly higher instantaneous power consumption than VANICP across most models. However, since our strategy achieves shorter runtimes, its overall energy efficiency surpasses that of VANICP for all models except *Bookshelf* and *Bunny*, resulting in energy savings between 16.4% and 58.63%.

Table 2 presents the results of comparing existing methods across multiple mobile platforms. FRICP demonstrates excellent efficiency on the small-scale *ModelNet* dataset, significantly outperforming embedded GPU-based approaches. However, its performance degrades as the dataset size increases. Among the embedded GPU methods, our strategy achieves performance comparable to VANICP and attains nearly twice the speed of the remaining methods. It is also worth noting that we include experimental results on an FPGA platform, which achieves the highest speed among all methods. However, its accuracy is lower due to the use of integer-based processing.

## 5 Related Work

In recent years, numerous studies have focused on accelerating the processing of the ICP algorithm through various approaches to promote the practical applications of point cloud technology.

Zhang et al. treated the classic ICP algorithm as a Maximization-Minimization (MM) algorithm [15], using Anderson acceleration to speed up the algorithm’s convergence. This approach reduces the number of iterations to improve the algorithm’s processing speed and minimizes the error parameters based on the Welsch function introduced in the method. Li et al. used a K-D tree [17] data structure to organize scattered point cloud data, improving the efficiency of nearest neighbor search in the algorithm. However, the K-D tree-based search process requires a large number of non-continuous memory accesses, placing high demands on memory bandwidth. In [18], the authors proposed a hierarchical graph-based KNN search method and the corresponding hardware sorting network to accelerate the ICP algorithm. This method organizes data points into a graph structure with multiple hierarchical levels, achieving faster and more efficient searches by progressively narrowing the search space, which offers a significant advantage over traditional K-D tree search methods. Li, Zheng, and Xiao, based on an approximate K-D tree structure, proposed an efficient parallel sorting circuit [19] to accelerate the sorting of large amounts of data during tree construction, while simultaneously computing the Euclidean distances of all points in the subspace. However, this approximate K-D tree-based method is prone to finding incorrect nearest neighbor target points, which leads to the ICP algorithm requiring more iterations. In [20], Wang et al. proposed an improved Local Sensitive Hashing (LSH) method, which can assign



similar points to the same hash bucket (low-dimensional space), thereby reducing the search space and accelerating kNN search speed. This method requires the selection of an appropriate hash function to ensure that similar points are assigned to the same bucket. In [21], the authors designed multiple units to store point cloud data. These units perform parallel nearest neighbor searches, and the sum of the absolute differences in the coordinates of the source and target points in three dimensions replaces the traditional Euclidean distance calculation. This method of using the sum of coordinate differences instead of Euclidean distance calculation may lead to larger errors and increase the number of iterations of the algorithm.

## 6 Conclusion

In this work, we introduced an embedded GPU-oriented ICP accelerator for point cloud registration. The proposed strategy employs a dynamic memory assignment strategy that adapts to the point distribution within each voxel block, substantially reducing memory consumption. Moreover, by integrating a voxel-wise dilation scheme, the accelerator converts global nearest-neighbor queries into localized searches, effectively lowering computational demands without compromising registration accuracy.

Looking ahead, we plan to enhance both the operational frequency and the precision of the accelerator, and to explore its applicability across a wider range of mobile computing platforms.

## References

- [1] Tom Roussel, Tinne Tuytelaars, and Luc Van Eycken. Unsupervised motion estimation of vehicles using icp. In *2021 IEEE International Conference on Robotics and Automation (ICRA)*, pages 7599–7605. IEEE, 2021.
- [2] Fahira Afzal Maken, Fabio Ramos, and Lionel Ott. Stein icp for uncertainty estimation in point cloud matching. *IEEE robotics and automation letters*, 7(2):1063–1070, 2021.
- [3] Ignacio Vizzo, Tiziano Guadagnino, Benedikt Mersch, Louis Wiesmann, Jens Behley, and Cyrill Stachniss. Kiss-icp: In defense of point-to-point icp—simple, accurate, and robust registration if done the right way. *IEEE Robotics and Automation Letters*, 8(2):1029–1036, 2023.
- [4] Paul J Besl and Neil D McKay. Method for registration of 3-d shapes. In *Sensor fusion IV: control paradigms and data structures*, volume 1611, pages 586–606. Spie, 1992.
- [5] Kenji Koide, Masashi Yokozuka, Shuji Oishi, and Atsuhiko Banno. Voxelized gicp for fast and accurate 3d point cloud registration. In *2021 IEEE international conference on robotics and automation (ICRA)*, pages 11054–11059. IEEE, 2021.
- [6] Kenji Koide, Masashi Yokozuka, Shuji Oishi, and Atsuhiko Banno. Globally consistent 3d lidar mapping with gpu-accelerated gicp matching cost factors. *IEEE Robotics and Automation Letters*, 6(4):8591–8598, 2021.
- [7] Alexander Agathos and Philip Azariadis. Multi-gpu 3d k-nearest neighbors computation with application to icp, point cloud smoothing and normals computation. *Parallel Computing*, 121:103093, 2024.
- [8] Ziyang Yu, Qiong Chang, and Jun Miyazaki. Fsc-ia: A hierarchical constructed sac-ia algorithm for point cloud alignment acceleration. In *2025 IEEE International Conference on Image Processing (ICIP)*, pages 1486–1491. IEEE, 2025.
- [9] Qiong Chang, Weimin Wang, and Jun Miyazaki. Accelerating nearest neighbor search in 3d point cloud registration on gpus. *ACM Transactions on Architecture and Code Optimization*, 22(1):1–24, 2025.
- [10] Weimin Wang and Qiong Chang. Van-icp: Gpu-accelerated approximate nearest neighbor search for icp registration via voxel dilation. In *ICASSP 2023-2023 IEEE International Conference on Acoustics, Speech and Signal Processing (ICASSP)*, pages 1–5. IEEE, 2023.
- [11] Michael Greenspan and Mike Yurick. Approximate kd tree search for efficient icp. In *Fourth International Conference on 3-D Digital Imaging and Modeling, 2003. 3DIM 2003. Proceedings.*, pages 442–448. IEEE, 2003.
- [12] Zhirong Wu, Shuran Song, Aditya Khosla, Fisher Yu, Linguang Zhang, Xiaoou Tang, and Jianxiong Xiao. 3d shapenets: A deep representation for volumetric shapes. In *Proceedings of the IEEE conference on computer vision and pattern recognition*, pages 1912–1920, 2015.
- [13] Greg Turk and Marc Levoy. Zippered polygon meshes from range images. In *Proceedings of the 21st annual conference on Computer graphics and interactive techniques*, pages 311–318, 1994.

- [14] Jürgen Sturm, Nikolas Engelhard, Felix Endres, Wolfram Burgard, and Daniel Cremers. A benchmark for the evaluation of rgb-d slam systems. In *2012 IEEE/RSJ international conference on intelligent robots and systems*, pages 573–580. IEEE, 2012.
- [15] Juyong Zhang, Yuxin Yao, and Bailin Deng. Fast and robust iterative closest point. *IEEE Transactions on Pattern Analysis and Machine Intelligence*, 44(7):3450–3466, 2021.
- [16] C. Sharma. Project4-cuda-icp. In *Online*, 2019.
- [17] Shihua Li, Jingxian Wang, Zuqin Liang, and Lian Su. Tree point clouds registration using an improved icp algorithm based on kd-tree. In *2016 IEEE International Geoscience and Remote Sensing Symposium (IGARSS)*, pages 4545–4548. IEEE, 2016.
- [18] Atsutake Kosuge, Keisuke Yamamoto, Yukinori Akamine, and Takashi Oshima. An soc-fpga-based iterative-closest-point accelerator enabling faster picking robots. *IEEE Transactions on Industrial Electronics*, 68(4):3567–3576, 2020.
- [19] Yiming Li, Kailei Zheng, and Hao Xiao. A knn accelerator based on approximate kd tree for icp. In *2022 International Conference on Image Processing and Media Computing (ICIPMC)*, pages 124–128. IEEE, 2022.
- [20] Chengliang Wang, Zhetong Huang, Ao Ren, and Xun Zhang. An fpga-based knn search accelerator for point cloud registration. In *2024 IEEE International Symposium on Circuits and Systems (ISCAS)*, pages 1–5. IEEE, 2024.
- [21] Shi Feng-Yuan, Zheng Xun-Jiang, Jiang Li-Hui, PAN Di, and LIU Bing. Fast point cloud registration algorithm using parallel computing strategy. In *Journal of Physics: Conference Series*, volume 2235, page 012104. IOP Publishing, 2022.